Moiré Interferometry Applied to Fracture in Titanium Tubes

P M. MacKenzie

Department of Mechanical Engineering, University of Strathclyde, Glasgow, UK

Abstract

Despite there being a substantial body of evidence to the contrary, moiré interferometry is often regarded – even by some adherents – as a curiosity of the optics lab. The present work seeks to demonstrate still further that the method can be an effective tool for practical materials research and assessment, in this case, in a novel and challenging experimental application involving fracture testing of heat exchanger tube material, the work being conducted in a conventional materials test laboratory setting. The key to the utility of the present setup lies with the priority given to its optical efficiency.

In standard fracture toughness tests, it is axiomatic that standard specimen geometries be used. A dilemma arises when a material's properties are transformed to a substantial degree by the final stages of its process of manufacture, and when the very nature of the finished form dictates that standard geometries cannot be produced. The focus of this investigation was to measure crack-tip opening displacements (CTODs) in thin-walled titanium tubes. Fringe patterns corresponding to in-plane displacement contours were obtained interferometrically and the method for extracting CTODs from these is described. Significant differences in yield, ultimate strength, elongation and fracture behaviour were observed for different material orientations.

Keywords: moiré interferometry; fracture mechanics; titanium; tubes; crack.

1. Introduction

Titanium and its alloys are well known to be established materials of choice in many aerospace applications where advantages in strength-to-weight and stiffness can make them more attractive economically than aluminium based counterparts. Titanium's exceptional resistance to corrosion and its resistance to crevice attack, coupled to its other characteristics, mean that it is also increasingly being used to good effect in specialist applications in relatively large scale items such as heat exchangers **[1]**. The present work dealt with thin-walled commercially pure (CP) titanium tubes of a type to be used in sea-water cooled condensers.

In its ductile α–phase (hexagonal close packed) condition, CP titanium can be rolled, drawn or extruded quite straightforwardly, although the textures so developed can have a marked effect on the mechanical properties of the finished item. Further, the presence of interstitially-soluble impurity elements, principally oxygen, nitrogen, hydrogen and carbon, has a marked effect on the material's mechanical properties, and with small increases in content, there is a substantial strengthening effect and, ultimately, pronounced embrittlement **[2].**

The aim of the work reported here was to demonstrate a technique for evaluating some key properties of finished thin-walled tubes. Certain common fabrication processes, such as roller expansion of tubes into tube-sheets, involve high levels of plastic deformation of the tube material and, to this end in particular, special interest was focussed on developing methods for assessing the response of the material in the hoop direction. Given the degree to which the mechanical properties of this material may be affected by the chemical composition and by the finishing process, it was the

purpose of this study to develop an approach which would, in principle, enable the evaluation of representative performance data for finished tubes.

2. Experimental Technique

2.1 Specimens

Chemical analysis gave the composition as stated in Table 1. The tubes were drawn to a wall thickness of 0.90 mm and then vacuum annealed and, as such, the ductility, strength and fracture toughness could not be presumed to be identical to those exhibited by any standard test specimens taken from the original extruded blank before it entered the drawing process. Figure 1 contains micrographs of the final grain structure of the finished tube showing it to be quite fine and equiaxed.

2.2 Hoop-stress Loading System

One objective of the work was to develop a system which could be used to compare, quantitatively, the ability of tubes of different composition and treatment to withstand the gross deformation applied in the fabrication process of fixing tubes to tube-sheets. Conventionally, tubes are fixed to their tube-plates by being plastically expanded into the holes in the plate. The expansion process also causes plastic deformation of the tube-plate in an area restricted to the vicinity of the hole. Forces required for sealing and for mechanical fixing of the tubes in position are thus provided by the elastic far field compressive stresses left behind as a consequence of the plastic deformation. Methods which are used for tube/tube-plate expansion include mechanical rolling using a special tapered mandrel and rolling tool, and hydraulic expansion, much of the tube deformation taking place as it expands to take up the initial gap between tube and plate. (The work by Goodier and Schoessow **[3]** remains the principal theoretical

underpinning for this process.)

In the mechanical rolling process, the tube is unconstrained in the axial direction and, partly for this reason, a loading system was designed such that hoop stresses could be applied, giving circumferential expansion only, and axial loads during testing could be eliminated or at least minimised. With a view to future applications on tubes in which there may be significant anisotropy in texture, it was also felt desirable to have the facility to evaluate the axial and hoop performance separately. Whilst axial testing could be performed straightforwardly, a hydraulic pressurising system had to be manufactured for the latter purpose.

The hydraulic test rig was designed to perform two main functions: to ensure loading of the specimens in the desired manner, i.e., no axial loading; and to enable controlled application of the loading or expansion. Specimens of dimensions given in Figure 2 were mounted on a steel core, through which the pressurised hydraulic oil was delivered; the core also supported the tube-sealing arrangement. In order to eliminate axial loads, it was essential that the tubes be free-floating, i.e., the ends could not be plugged during the tests. A setup using conventional 'O'-ring seals in tandem with PTFE backing washers (to prevent seal extrusion) was adopted (Figure 3).

The pump unit, which also incorporated the specimen holder, is shown schematically in Figure 4. A key feature of the design is that the pressure end-loads imparted through the specimen cores were supported by, on the one hand, the pump body, and on the other, by the retaining cross-head mounted on reaction columns. By using two-piece cores, a potential problem in the oil-way at the core to body seal was eliminated

since it was possible, by selecting appropriate dimensions, to ensure that the outward hydraulic force tending to open the seal was always more than balanced by the pressure force on the core from within the specimen.

Controlled application of pressure within the system was achieved by designing it to be mounted between the platens of an Instron 1342 general purpose servo-hydraulic testing machine.

Prior to each test, the hydraulic system, including the fresh specimen, was recharged with working fluid (Esso Nuto-H46) by first evacuating it to ensure no air pockets remained.

2.3 Tensile Stress Loading

Tensile loading of the specimens was by comparison, a simple business of reinforcing the tube ends and loading the specimens in the same test machine in its standard setup. Specimen tube lengths of 350 mm were used in this part of the investigation.

2.4 Stress-strain Testing

As a first stage in the assessment, the stress-strain characteristics of the material in the drawn, annealed condition were to be evaluated. Given, also, that a significant part of the study was to be focussed on the circumferential direction, stress-strain testing to failure was conducted using the hydraulic pressurising system described above.

A calibrated transducer was used to measure directly the pressure applied to the tube in the hydraulic tests. In this case, strain measurements were derived from a clip

gauge modified to measure the diametrical expansion of the specimen. Both sets of readings were logged electronically; four specimens were tested for each orientation.

Axial testing to failure was conducted in a conventional tensile test setup, loads being obtained from the test machine load cell and displacements measured on a 50 mm gauge-length using a displacement transducer. Elongation over the point of failure was measured using pre-marked scales on the specimens over an initial gauge-length of 50 mm. The measurement procedure mirrored the prescription of **[4]** for tensile testing of tubes. Similarly, the loading method followed the standard, the tensile forces being applied through reinforced tube-ends, these taking the form of close-fitting hardened steel inserts 75 mm in length. The specimen ends were clamped in hydraulically operated V-block jaws; in order to minimise bending effects, the lower of the two gripping assemblies, i.e., on the test machine actuator, was arranged to be conveniently adjusted for axial alignment only *after* the gripping forces had been applied.

Summary results for both loading configurations are presented in Table 2. The gross change in shape of the hoop loaded specimens at failure means that the pure hoop loading condition has been nullified and elongation results should be treated with caution for this reason alone, as should the comparisons between values of Ultimate Stress. However, the 22% difference in Proof Stress can be accepted with confidence and the 54% difference in Ultimate Stress is still worthy of notice, albeit with a caveat attached.

2.5 Preparation and Pre-cracking of Fracture Specimens

Starter notches for both axial and circumferential configurations were produced by machining a slot using a 1.5 mm slitting saw set up in a milling machine.

In order to perform the fracture testing of the material for the hoop loading setup, it was necessary to devise a method for both pre-cracking and, finally, testing, the tube whilst at the same time maintaining hydraulic integrity of the apparatus. This was achieved by using a slightly modified core which had its diameter reduced so as to be able to accommodate a sheath of heat shrink material to provide a hydraulic seal over the notch, overlaid with a sleeve of 0.1 mm thickness steel shim to prevent the sealing sheath from being extruded through the notch. In Figure 3, one can see an undercut of 2 mm between the ends of the sealed section on the two-part core and it was onto this that the sheath material was attached. The stepped ends to the undercut prevented the sheath material from extruding into the 'O'-ring sealing area of the core. As the polymeric sealing sheath was of negligible strength and stiffness compared to the test material, it was reasonable to assume that its presence would have no significant strengthening effect. The shim would tend to reduce the local bulging in the vicinity of the notch but it would not carry any of the hoop loading as it was entirely free to float at each of its edges, and, in addition, the sheath-to-shim-to-tube interfaces were lubricated.

No fatigue data were readily available for the material in the form tested and the following was found to be satisfactory after some trial work. Pre-cracking for the hoop stress case consisted of applying 20,000 applications of a loading range of 0.3 to 2.0 kN to the hydraulic pump, followed by 70,000 cycles at 0.3 to 1.2 kN. The range of applied stress intensity factors, ΔK , was obtained from:-

$$\Delta K = Y\Delta\sigma\sqrt{\pi a} \quad (1)$$

where a was the crack length, $\Delta\sigma$ was the stress range, and Y was a geometric factor to take account of the configuration of the crack in relation to the applied stresses.

The compendium of stress intensity factor solutions for cracked tubes provided in **[5]** can be drawn on to obtain values for Y, so enabling this loading regime to be equated, approximately, to an initial stress intensity range of K = 2.2 to 14.4 MPa $m^{1/2}$ for a notch length of $2a$ = 4.3 mm, reaching K = 4.4 to 17.4 MPa $m^{1/2}$ for a final fatigue crack length of $2a$ = 8.3 mm. The characteristics of the equipment were such that a loading frequency of only 1 Hz could be applied.

The crack specimen for tensile loading was loaded at 2.5 Hz through 120000 cycles from 0.2 to 1.5 kN, the initial notch being 10 mm long, growing to 13.2 mm at the end of fatigue treatment. Again, the appropriate solution provided in **[5]** can be used to evaluate the applied stress intensity range which was 1.4 to 10.7 MPa $m^{1/2}$ to begin with, rising to 2.2 to 17.1 MPa $m^{1/2}$ for the final length of the fatigue crack.

On completion of the fatigue pre-cracking sequences, a 1.5 mm diameter hole was drilled at one end of the crack, removing the sharp tip, in order to inhibit further growth in these areas during the fracture test to come, thereby allowing attention to be focussed on the remaining crack-tips. Finally, the effective crack lengths in both specimens were measured in the loaded condition using a travelling microscope: $2a$ = 8.8mm for the axial crack; $2a$ = 13.7mm for the circumferential crack.

2.6 Moiré Interferometry

Moiré interferometry has evolved into a highly productive technique for evaluating a variety of material properties in circumstances where fine spatial discrimination and accurate strain and/or displacement information are required, making it especially suitable for many experimental studies in fracture research **[6].**

The details of the variations in technique and optical equipment used in the technique have been described at length elsewhere **[7,8,9]** but some of the essential elements, as they apply to this investigation, may be discussed quite briefly.

Central to the method is the application of an optical diffraction grating applied over the area of interest on the test specimen. With all moiré measurement methods, system sensitivity is directly linked to the grating frequency such that, *U*, the component of in-plane displacement at right angles to the grating lines is given very simply by:-

$$U = N\,p \tag{2}$$

where *N* is the number of fringes of fringes or fractional fringes separating two points and *p* is the pitch of the reference grating which, in the case of interferometric moiré, can be considered to be a ”virtual” grating formed in the overlap of two coherent, collimated beams (Figure 5). The pitch, *p*, of the virtual grating is obtained from simple geometry and is dependent on the wavelength of light utilised, λ, and the enclosed angle, Φ :-

$$p = \frac{\lambda}{2\sin\Phi/2} \tag{3}$$

In the case of the present study, a 475 lines/mm grating was formed in epoxy resin (Emerson & Cuming - Stycast 2057) on the surface in the zone of interest using a replication technique **[10].** The pitch of the undeformed specimen grating must be

identical to, or an exact integer multiple of, the pitch of the reference grating in order to produce an initial null fringe field.

An important feature of the setup was the attention paid to optimizing the optical efficiency, so enabling its use in a normal materials test lab, rather on a vibration isolated optical table. One factor in this was that the master grating from which the replicas were taken was produced using a "blazing" process **[11]**, resulting in the cross-sectional profile of the grating structure being of a particular chosen shape. The desired consequence of this was that the available light directed onto the specimen was returned preferentially in the diffracted orders which were to be imaged and recorded for analysis. By adding green dye to the grating resin, fringe contrast was protected from the damaging effect of the proportion of incident light which would otherwise pass through the grating and back-scatter from the substrate surface.

The present work was an unusual application for moiré interferometry in that the specimen grating had to be applied to a surface with a very significant degree of curvature. Grating material was cast onto the tube surface to form a flat, and onto this, the grating itself was then replicated. This could have been a source of problems if fringe information had been required from areas having a thick substrate but care was taken to ensure that the flat was tangential to the area of interest around the crack-tip and thus the substrate material was sufficiently thin here (about 0.05 mm) to exhibit minimal shear lag between the specimen surface and the surface of the grating; in other words, in the zone in which one would be interested, the grating thickness was kept to a minimum and, therefore, the information transmitted through the grating would, for this application, be an adequately good representation of specimen

behaviour.

The deformation of the grating was monitored using one of the portable interferometers developed at Strathclyde (Figure 6). The light source was a helium-neon laser of 12 mW polarized output at 632.8 nm wavelength; the output beams were collimated and expanded to 50 mm diameter, this, therefore, being the approximate maximum field of view of the system. The interferometer consists of a system of mirrors and beam-splitters set in a fixed geometry and arranged to give three output beams which emanate from the plane of the instrument at mirrors M1, M2 and M3. These beams impinge on the specimen grating at precise angles so that the diffracted orders returning through the collector lens are, for an undeformed grating, exactly parallel to each other and normal to the plane of the specimen diffraction grating. Where the grating has been deformed, the light rays will be redirected away from the "zero field" condition and, by combining a pair of return orders, one can observe interference between the two, the degree of interference in any part of the image being in direct proportion to the change in pitch of the grating induced by the deformation.

In order to enable maximum use to be made of the available light, all of the optical elements within the instrument were individually coated so as to optimise their performance, taking account of the particular function and location of each in their respective beam path. It was crucially important to ensure that the design of the layout was configured so as to maintain identical polarization angles for the light returning to the imaging system for each of the three diffracted orders in use. Finally, in order to maximize the proportion of light available for coherent interference between the beams, the optical path length of each of the three outputs, measured from the source,

was made to be identical ±1mm (coherence of light beams split from a common He-Ne source shows progressive deterioration as path length difference increases, reducing to an unusable level at differences of about 200-300 mm).

As stated already, the sensitivity of the system, in relation to the grid pitch of 1/475 lines/mm, is doubled optically by using the virtual reference grating of 950 lines per mm**.** Consequently, the interferometer reveals fringe patterns which are contours of constant in-plane displacement with a contour interval of 1/950 mm. Although the arrangement used here allows for three output beams to be used to interrogate a specimen grating to observe displacement fields at 0°, 45° and 90° to the axis of the cross-grating, only one component was required for the present study. The high efficiency of the system enabled the fringe patterns to be recorded by conventional photography using a Contax RTS SLR camera and 35 mm Kodak Tri-X 400 film.

2.7 Data Reduction and Accuracy

In the vicinity of an opening crack, the fringe patterns revealing the displacement component parallel to the direction of opening are relatively easy to assess with only a little experience of interferogram analysis. As already stated, the contour interval, or fringe-sensitivity, was, for the setup used here, 1/950 mm. Quite simply, each point along any fringe centre has been displaced along the component of interest by one interval from every point on the centre of the adjacent fringe, two intervals from the next fringe, and so on. It follows then that, for the upper and lower faces of an opening crack, as, for example, in Figure 7, the displacement induced between two points can be measured precisely by counting the number of fringes separating each, along the crack edges and around the crack-tip, and multiplying this by the fringe

sensitivity. Thus we can see that the two points, A and B, are separated by 41 complete fringe pitches and, for the setup geometry used here, this equates to 43.2 microns of displacement between those points on the crack face. By plotting fringe count against fringe position measured from the crack-tip, we can, therefore, obtain an accurate representation of the crack opening shape in profile.

Although a good deal of effort has been devoted towards developing automated systems for analysing fringe patterns, these are not without drawbacks **[12]** and for work such as that reported here, a simple semi-automatic approach has been found to be accurate, repeatable and efficient **[13].** This was based on a graphics tablet linked to a desk-top computer, data such as fringe centres and scaling fiducials being identified manually and entered into the system through the tablet's cursor, the computer being used both to log the results, perform scaling arithmetic and finally, data reduction. Analysis work was carried out on photographic prints enlarged to 250 x 200 mm for the area of interest in the vicinity of the crack (in other words, a magnification factor of approximately 40).

As already stated manual identification of the centres of half-fringes, i.e., black or white, has been shown to be a procedure which is accurate and repeatable. The basic increment of discrimination, one half fringe, equates to a displacement of 1/1900 mm. In general terms, based on previous assessments, we could claim, therefore, that the displacement measurements of the present work are in increments of 1/1900 mm, readily identifiable and accurate to within a quarter fringe, in other words, $\pm$ 0.26 microns. However, particularly at higher load points, there are areas where the fringe density is very high and, in such circumstances, it is estimated that an accuracy of one

fringe, or 1.05 microns, should be assumed. Applying the latter conservative estimate, we still have a degree of accuracy which was adequate for this application.

Spatial resolution, which, for our purpose, we will define as the degree to which a particular data value can be related to a physical position on the specimen, is an important issue which interacts with fringe sensitivity and accuracy in problems such as these. This is a matter which is influenced by a variety of factors including the characteristics of the optics, the photographic procedure and the scale of the enlarged image of the interferogram, together with, in this case, the limitations of the digitising hardware **[14]**. For this study, it was estimated to be 0.1 mm.

3. CTOD Measurement from Moiré Interferograms

Referring again to Figure 7, a relatively noise-free example of a typical fringe pattern one would observe in an opening-crack displacement field, we are presented with a wealth of data relating directly to the deformed geometry of the material surrounding the crack.

In order to make use of the information, it is necessary to proceed as follows. First of all, a fringe number, zero, is assigned to the fringe emanating from the crack-tip and parallel to it. Systematically those fringes above the crack are then numbered in ascending order and those below in descending order. Each fringe is a contour of in-plane displacement, and, for the arrangement used here, the displacement component recorded is normal to the crack. It follows quite simply that, where a fringe intersects with the crack, it defines the displacement value which can be attached to that

location. By plotting displacement against position along the crack, and repeating this over a range of loadings, one can observe the development of the profile of the crack as it opens.

Interferograms were recorded for a range of applied hoop stresses up to 205 MPa, and for the axial loading configuration, to a maximum of 114 MPa. Figure 8 shows representative samples of the fringe patterns obtained for each condition.

As an example of some of the detail which may be obtained using this technique, the crack profile for the data extracted from Figure 8(a) (hoop-load and longitudinal crack) is presented in Figure 9, together with the value obtained for CTOD. At all load points for this configuration, there was some evidence of spurious fringe information close to the edge of the crack, this being due to a small amount of out-of-plane bulging caused by the internal pressure; normally, this zone contains the loci from which fringe data would be obtained for crack profile evaluation. The moiré system is intolerant of substantial localised changes in grating slope and therefore, instead, fringe information at a distance of 0.5 mm from each side of the crack edge was used in the analysis. In Mode I crack opening, which is essentially what we have here, this approach is assumed not to have introduced significant errors. For consistency, the same approach was used in analysing the fringe patterns obtained for the axial load case (though, here too, there was some evidence of out-of-plane displacement near to the crack edges, especially at higher stress levels).

4. Results and Discussion

Figures 10(a) and 10(b) illustrate the development of CTOD with increasing stress

applied to the tube for the hoop loaded and axially loaded specimens respectively. In line with the recommendations in the standard test method **[15]**, measurements were base on an assumption that the crack tip was stationary throughout, i.e., blunting and crack extension were ignored and opening displacements are for a position fixed on the tip of the original fatigue crack. A feature of the standard test which can present some difficulties but which could be avoided in the present case was the need to assign a rotation factor in order to be able to interpret readings from clip gauges of displacements remote from the tip itself. For the standard single-edge notch specimen geometry, a nominal position of 0.4 of the remaining ligament ahead of the crack has been chosen, but even with a standard specimen, experimental values have been reported in the range 0.33 to 0.49. The tube specimen tested here is distinctly non-standard but for the purpose of obtaining δ, the moiré fringe data enabled a true rotational hinge-point to be determined straightforwardly for each load step.

Drawing, again, on the standard test for guidance in the procedure for determining significant deltas values, we have two possibilities: the value of CTOD, δ_C, at the onset of crack extension; or the value, δ_M, observed on reaching the maximum force plateau. Crack growth was not measured during the test and so the former option was not available (nor was pop-in observed).

Dealing first of all with Figure 10(a) (hoop loading) there is quite clearly a stress plateau. A least-squares fit is shown for the elastic loading line (together with the 95% confidence bands). The standard states that the value for the plastic component of CTOD, δ_P, may be prescribed to be that obtained when the elastic component, δ_E, has been subtracted from δ_M. This can be evaluated graphically as shown in the

figure.

The axial load test results in Figure 10(b) show a very different type of behaviour. For comparison, line AB, parallel to the elastic loading line, has been drawn through the value of δ_P previously measured in Figure 10(a) for the hoop loaded specimen. Whereas a load plateau was apparent in Figure 10(a), this was not encountered within the range of the moiré measurement system for the axially loaded crack; instead, the material appears to show a steeply rising resistance to fracture.

A more appropriate comparison can be made by drawing again on the cracked tube linear elastic solutions from **[5]** together with the appropriate solution for the applied stress intensity factors, K_{APP}, for the various load points of interest in relation to CTOD values. Thus:

$$K_{APP} = Y\sigma_{APP}\sqrt{\pi a} \qquad (4)$$

where σ_{APP} is the applied stress, remote from the crack, Y is a geometric factor as described earlier, and a is the crack length.

The results are summarised in Table 3. Referring to Figure 10(a) and the first row of the table, we take the characteristic results for the axial crack, i.e., K_M, δ_M, and δ_P, as the baseline reference values for our comparisons throughout. (These baseline values are flagged at all points where they appear in the table.)

Thus, taking the observed maximum value of stress for the axial crack, the "applied" stress intensity factor was K_M = 55 MPa $m^{1/2}$. This applied K value produced a measured maximum CTOD of $\delta_M = 46$ microns. By comparison, referring to the

immediately adjacent data in the table, and to Figure 10(b), one can see that with an identical level of "applied" stress intensity factor, K_{APP} = 55 MPa $m^{1/2}$, the circumferential crack would experience a very much larger CTOD of δ = 96 microns

.

Turning now to the comparison summarised in next row of the table, we are here using as the reference baseline δ_P (the plastic component of CTOD), which was measured for the axial crack using the data in Figure 10(a) and following the method prescribed in **[15]**, to give δ_P = 32 microns. Referring now to Figure 10(b), if we project a line, **A-B**, parallel to the elastic loading line and passing through a "notional" δ_P = 32 microns, we can see that, for this amount of plastic CTOD, the circumferential crack supports a stress which corresponds to K_{APP} = 43 MPa $m^{1/2}$, i.e. significantly lower than the baseline axial K_M of 55 MPa $m^{1/2}$; also, for this notional δ_P, the circumferential crack exhibits a very much higher total δ of 62 microns.

Finally, taking, for the axial crack, the observed δ_M of 46 microns as per **[15]**, we can see that the load required to produce a CTOD of this magnitude in the circumferential crack generates a value of K_{APP} of 38 MPa $m^{1/2}$ (compared with the baseline 55 MPa $m^{1/2}$).

The evidence is quite conclusive that there were significant differences in the observed fracture performance between cracks similarly loaded (i.e. Mode I opening) but 90° apart in orientation. The primary objective of the work was to develop a method of applying high-sensitivity moiré to this type of fracture problem and, although this has now been clearly demonstrated, one must go on to speculate as to

the causes of the observed differences.

First of all, and most probable, are the mechanical effects arising from metallurgical features of the tubes. The essence of the anisotropic plastic and fracture properties frequently observed in α-titanium lies with the properties of the hexagonal unit cell and the geometrically limited ability of this to allow slip. The orientation of such cells is therefore crucial in determining the behaviour of the material on the macro scale. The material here had certainly been annealed but although samples of its microstructure were observed to be fine-grained and equiaxed, these facts alone are not sufficient to ensure three-dimensional isotropic texture; unfortunately, a detailed metallurgical study of the three-dimensional structure was beyond the scope of this investigation. However, the effects on texture and sub grain-scale features arising from processes involving cold-working and annealing of α-titanium have long been regarded as complex **[2, 16,],** and this is an area which continues to be the subject of research by materials scientists, as exemplified by **[17,18].** Indeed, the anisotropy induced by such processes is now being tailored to suit particular component applications in order to exploit the advantageous fatigue resistance of particular orientations **[19].** In summary, according to Polmear **[20],** the combination of cold-working and heat-treatments typically applied to CP titanium "may cause changes to fine scale features of the micro-structure, but little is known of these effects."

The question of crack-tip constraint is always of primary concern in a fracture mechanics. However, since we are here dealing with material in its final, full-scale, thin-walled condition, the notion of satisfying a plane strain fracture condition, such as would be required in standard LEFM tests, is not an issue. In order to ensure that

constraint conditions during tests are appropriate, the British Standard **[15]** prescribes that for CTOD tests, the specimen material shall be of the thickness of the material application of interest; for both crack orientations in the present work, the wall thicknesses were identical and therefore satisfied this element of the requirement. An item not dealt with in test standards is the effect of anisotropic yield behaviour on crack-tip plastic zone development and this will consequently influence crack-tip constraint to some degree. In the present case, the measured values of Proof Stress differed between orientations by 22%, and this must be regarded as significant. However, for the very reason that the anisotropic yield may influence the constraint for different orientations of crack, one might justify assessing such tubes in this way as, individually, the constraint conditions are entirely realistic for the respective crack orientations, albeit they may differ from one to the other. (Recalling too, that the method described here is not proposed as a technique for measuring a material property; rather it is intended for evaluating material response in its finished manufactured form).

The possibility of spurious bending loads being applied in the axial loading case was taken heed of during the tensile testing of the tubes, and similarly in the tensile loading of the cracked specimen. Additionally, the ability to view the interferometric fringe patterns in real-time, from the moment the cracked specimen has been attached to the test machine, and thereafter throughout the test, provides the experimentalist with immediate, and very obvious, feedback regarding the presence of any misalignment or of off-axis strains. In this investigation, therefore, the possibility of spurious bending loads influencing the observed CTOD measurements can be eliminated.

5. Conclusions

A system has been constructed for circumferential load testing of ductile, thin-walled commercially pure titanium tubes, axial loading being eliminated. In conjunction with experimental techniques based on moiré interferometry, this enabled a process for measuring a fracture characteristic, namely crack-tip opening displacement, to be demonstrated. For the purpose of comparison, tube specimens of the same material were tested under axial loading, the fracture performance also being revealed using the moiré method. Differences in crack resistance characteristics were observed for the two crack orientations. Testing to failure of uncracked tubes showed that, between the two orientations of loading, there were significant differences in Proof Stress, Ultimate Tensile Stress and Elongation. It is reasonable to speculate that the texture introduced during the tube manufacturing process may have been a factor in causing such differences and the literature substantially confirms this. Optical microscopy showed the grain structure to be apparently equiaxed but comprehensive assessment of texture could not be observed using this technique alone.

The moiré setup described here was an appropriate tool for the fracture component of this particular investigation but some limitations of a general sense can be anticipated. The fixed-geometry high-sensitivity configuration used here has been shown to have exceptional range **[7]** – up to 13% strain – and can, in principle, accommodate much larger displacements, such as would be expected of more ductile materials, or for work related to a more extensive degree of crack resistance. However, in order to achieve this, the interferometer must be re-adjusted to give a new null field at stages in the loading sequence when the divergence of the diffracted beams overtakes the

collecting capacity of the imaging system (in other words, when the situation corresponds to very high levels of fringe density). Such procedures were not utilised in the present work and, whilst this stepwise approach is an entirely practicable tactic for extending the range well beyond that used here, it lacks somewhat in convenience. On the other hand, a less sensitive system having considerably greater range but being of adequate displacement-sensitivity for this type of application could be constructed using identical optical principles. Also, it was found that localised out-of-plane distortions of the grating corrupted fringe data close to the crack edges; it is possible to devise optical methods by which this could be evaluated and accounted for but, for the purpose of the present work, a simpler process by which dependable fringe data were extrapolated was adequate.

Whilst one would not propose that the involved approach described here be adopted as a standard test method, it does, nevertheless, enable insight to be gained into a somewhat intractable area of materials assessment and investigation.

Acknowledgements

Grateful thanks are due to Mr J Sivewright and to Mr J Kelly for their sagacious technical assistance in support of this work.

References

1) Titanium Information Group, Titanium for Marine and Offshore Applications – A Designers' and Users' Handbook, Institutt for Energiteknikk, Kjeller, Norway, 1999.
2) Jaffee, RI, Promisel, NE, (eds), The Science, Technology and Application of Titanium, Pergamon Press, Oxford, UK, 1970.
3) Goodier, JN, Schoessow, GJ, The holding power and hydraulic tightness of expanded tube joints: analysis of the stress and deformation, *Trans ASME*, 1943, 65, 489-96.
4) BS EN 10002 - 1:2001, Metallic materials – tensile testing, British Standards Institute, 2001.
5) R6, 2001. R6: Assessment of the integrity of structures containing defects, Revision 4, British Energy Generation Ltd., UK, 2001
6) Walker, CA, (Ed), Handbook of Moiré Measurement, Institute of Physics Publishing, Bristol, UK, 2004.
7) McKelvie, J, Walker, CA, MacKenzie, PM, A workaday moiré interferometer: conceptual and design considerations, operation, applications, variations, limitations, Proc SPIE, Int Conf on *Photomechanics and Speckle Metrology* (San Diego CA), 1987, Vol 2, Bellingham WA: SPIE, 464-75.
8) Post, D, Moiré interferometry at VPI & SU, *Experimental Mechanics*, 1983, 23, 203-210.
9) Walker, CA, A historical review of moiré interferometry, *Experimental Mechanics*, 1994, 34, 281-299.
10) Walker, CA, McKelvie, J, A practical multiplied moiré system, *Experimental Mechanics*, 1978, 18, 316-320.

11) Hutley, MC, Diffraction Gratings, Academic Press, New York, US, 1982

12) McKelvie, J, On moiré interferometry and the level of detail that it may legitimately reveal, *Optics & Lasers in Engineering*, 1990, 12, 81-89.

13) MacKenzie, P, The influence of errors in an interferogram analysis, *Experimental Mechanics*, 1994, 34, 243-248.

14) McKelvie, J, Micro-scale strain measurement: limitations due to restrictions inherent in optical systems and phase-stepping routines, 485-498, in Handbook of Moiré Measurement, op cit.

15) BS 7448-1: 1991, Fracture mechanics toughness tests – Part 1: Method for determination of K_{Ic}, critical CTOD and critical J values of metallic materials, British Standards Institute, 2002.

16) Sullivan, TL, Texture strengthening and fracture toughness of titanium alloy sheet at room and cryogenic temperatures, NASA Technical Note TN D-4444, NASA, Washington DC, US, 1969

17) Bache, MR, Evans, WJ, Randle, V, Wilson RJ, Characterisation of mechanical anisotropy in titanium alloys, *Materials Science and Engineering*, 1998, A257, 139-144.

18) Hayama, AOF, Sandim, HRZ, Annealing behaviour of coarse-grained titanium deformed by cold-rolling, *Materials Science and Engineering*, 2006, A418, 182-192.

19) Bache, MR, Processing titanium alloys for optimum fatigue performance, *International Journal of Fatigue*, 1999, S105-S111

20) Polmear, IJ, Light Alloys: Metallurgy of the Light Metals, (3rd edition), Edward Arnold, London, UK, 1995.

APPENDIX

Notation

a	Crack length
K	Stress intensity factor
K_{APP}	Linear elastic applied stress intensity factor
K_M	Stress intensity factor at load plateau
N	Fringe count
p	Grating pitch
U	Displacement
Y	Geometric factor
δ	Crack-tip opening displacement
δ_E	Elastic component of crack-tip opening displacement at load plateau
δ_M	Crack-tip opening displacement at load plateau
δ_P	Plastic component of crack-tip opening displacement at load plateau
Φ	Included angle of intersecting beams
λ	Wavelength of light beam
σ	Applied stress

List of Figures and Captions

Figure 1: Micrographs of the grain structure of the titanium tube.

Figure 2: Dimensions of specimens used in pressurised tests. The axial starter notch for the fracture specimen was positioned centrally as shown in the diagram.

Figure 3: Split core sealing arrangement for pressurising tubes.

Figure 4: Schematic of specimen pressurising system consisting of a self-contained pump and specimen holder.

Figure 5: Virtual grating formed in the intersection of two coherent, collimated beams.

Figure 6: The Strathclyde design of moiré interferometer.

Figure 7: Example of a crack-tip displacement field. The fringes are contours of constant in-plane displacement for the displacement component at right-angles to the crack.

Figures 8(a) and 8(b)

a) Interferogram showing contours of the in-plane displacement component normal to the crack (162 MPa hoop-stress loading condition – axial crack).

b) Interferogram showing contours of the in-plane displacement component normal to the crack (100 MPa axial-stress loading condition – circumferential crack).

Figure 9: Example of a crack opening profile obtained from an interferogram, in this case, the fringe pattern depicted in Figure 8(a).

Figure 10(a) and 10(b):

a) Applied stress v. crack-tip opening displacements (hoop-stress loading condition).

b) Applied stress v. crack-tip opening displacements (axial loading condition).

MOIRE INTERFEROMETRY APPLIED TO FRACTURE IN TITANIUM TUBES

JMDA119

List of changes and response to referees.

1. *In response to the comments of Referee No.1 regarding the influence of material processing , grain structure, etc., viz:*

"My reading is that the tubes were cold drawn and annealed and so in the annealed condition would the authors expect to see a significant difference in toughness in the two orientations tested. There does not appear to be a significant grain orientation in the axial direction observed as a result of the cold drawing process."

I have included a substantial additional paragraph in the Discussion, speculating as to the likely influence of metallurgical factors as a cause of the observed anisotropic behaviour of the material along with five additional references to support the hypothesis thus:

ADDITION:-

First of all, and most probable, are the mechanical effects arising from metallurgical features of the tubes. The essence of the anisotropic plastic and fracture properties frequently observed in α-titanium lies with the properties of the hexagonal unit cell and the geometrically limited ability of this to allow slip. The orientation of such cells is therefore crucial in determining the behaviour of the material on the macro scale. The material here had certainly been annealed but although samples of its microstructure were observed to be fine-grained and equiaxed, these facts alone are not sufficient to ensure three-dimensional isotropic texture; unfortunately, a detailed metallurgical study of the three-dimensional structure was beyond the scope of this investigation. However, the effects on texture and sub grain-scale features arising from processes involving cold-working and annealing of α-titanium have long been regarded as complex **[2, 16,],** and this is an area which continues to be the subject of research by materials scientists, as exemplified by **[17,18].** Indeed, the anisotropy induced by such processes is now being tailored to suit particular component applications in order to exploit the advantageous fatigue resistance of particular orientations **[19].** In summary, according to Polmear **[20],** the combination of cold-working and heat-treatments typically applied to CP titanium "may cause changes to fine scale features of the micro-structure, but little is known of these effects."

2.

"Could the authors comment on the elimination of possible bending loads during the tensile tests on the tubes?"

I have inserted two additional pieces to account for this. First of all, in the section describing the axial tensile testing:

ADDITION:-

The measurement procedure mirrored the prescription of **[4]** for tensile testing of tubes. Similarly, the loading method followed the standard, the tensile forces being applied through reinforced tube-ends, this taking the form of close-fitting hardened steel inserts 75 mm in length. The specimen ends were clamped in hydraulically operated V-block jaws; in order to minimise bending effects, the lower of the two gripping assemblies, i.e., on the test machine actuator, was arranged to be conveniently adjusted for axial alignment only *after* the gripping forces had been applied.

Also, in the Discussion, I have appended an additional paragraph to describe the precautions taken to avoid the introduction of bending in various stages of the work:

ADDITION:-

The possibility of spurious bending loads being applied in the axial loading case was taken heed of during the tensile testing of the tubes, and similarly in the tensile loading of the cracked specimen. Additionally, the ability to view the interferometric fringe patterns in real-time, from the moment the cracked specimen has been attached to the test machine, and thereafter throughout the test, provides the experimentalist with immediate, and very obvious, feedback regarding the presence of any misalignment or of off-axis strains. In this investigation, therefore, the possibility of spurious bending loads influencing the observed CTOD measurements can be eliminated.

3.

"Are the authors convinced that the crack tip constraint conditions are the same for both loading types. If not, this could be source of toughness variation."

This comment leads us into an interesting point is worthy of further study: the effects of anisotropic yield on crack-tip constraint. I have explained that, although the geometric requirements for standard plane stress fracture testing conditions appear to have been met, the anisotropic behaviour could give rise to differences in constraint. In a sense, that is one of the main justifications for the work. I have responded in the Discussion as follows:

ADDITION:-

The question of crack-tip constraint is always of primary concern in a fracture mechanics. However, since we are here dealing with material in its final, full-scale, thin-walled condition, the notion of satisfying a plane strain fracture condition, such as would be required in standard LEFM tests, is not an issue. In order to ensure that constraint conditions during tests are appropriate, the British Standard **[15]** prescribes that for CTOD tests, the specimen material shall be of the thickness of the material application of interest; for both crack orientations in the present work, the wall thicknesses were identical and therefore satisfied this element of the requirement. An item not dealt with in test standards is the effect of anisotropic yield behaviour on crack-tip plastic zone development and this will consequently influence crack-tip constraint to some degree. In the present case, the measured values of Proof Stress differed between orientations by 22%, and this must be regarded as significant. However, for the very reason that the

anisotropic yield may influence the constraint for different orientations of crack, one might justify assessing such tubes in this way as, individually, the constraint conditions are entirely realistic for the respective crack orientations, albeit they may differ from one to the other. (Recalling too, that the method described here is not proposed as a technique for measuring a material property; rather it is intended for evaluating material response in its finished manufactured form).

4.

"Typographical errors

Section 2.1, line 2: insert wall before thickness.
Section 2.2, line 32: insert by before the pump...
Section 4, line 33: Equation (1) is set for fatigue loading with ranges whereas reference here is to quasi static loading.
Section 4, line 45: Is there a word missing before this level..?"

These have been corrected.

5. *In response to the second referee's comments regarding Table 3:*

"1. It is not immediately clear what is the significance of the rectangles round some numbers in Table 3. This should be spelled out in the text."

I have rewritten the entire text relating to the table and adjusted the table itself, making it, I trust, more straightforward to follow.

6.

"2. It is not too clear how the plastic shrink film is disposed on the core. Perhaps it could be indicated by further description in the text, referring to Fig.3."

I have redrafted the text relating to this to be more explicit:
AMMENDED:-
This was achieved by using a slightly modified core which had its diameter reduced so as to be able to accommodate a sheath of heat shrink material to provide a hydraulic seal over the notch, overlaid with a sleeve of 0.1 mm thickness steel shim to prevent the sealing sheath from being extruded through the notch. In Figure 3, one can see an undercut of 2 mm between the ends of the sealed section on the two-part core and it was onto this that the sheath material was attached. The stepped ends to the undercut prevented the sheath material from extruding into the 'O'-ring sealing area of the core.
7.

"3. The author is too modest in his criticism of the moiré technique as he employed it, in terms of its range. In his Ref.7, strains are determined up to 13%, using the same optical system, by employing the

technique of "shedding fringes" in a controlled manner. While in the case of the opening crack the shedding could only be effective on one face, above or below, with fringe addition occurring on the other face, it would be feasible to shed fringes on one side and then the other in the controlled manner necessary, and thus extend the range without losing the sensitivity. Reviewer thinks that an indication of this extension of range should be given, less the readership be left with a false impression."

Relaxing my inbuilt reticence, I hope, adequately, I have redrafted the section thus:
AMMENDED:-
The moiré setup described here was an appropriate tool for the fracture component of this particular investigation but some limitations of a general sense can be anticipated. The fixed-geometry high-sensitivity configuration used here has been shown to have exceptional range **[7]** – up to 13% strain – and can, in principle, accommodate much larger displacements, such as would be expected of more ductile materials, or for work related to a more extensive degree of crack resistance. However, in order to achieve this, the interferometer must be re-adjusted to give a new null field at stages in the loading sequence when the divergence of the diffracted beams overtakes the collecting capacity of the imaging system (in other words, when the situation corresponds to very high levels of fringe density). Such procedures were not utilised in the present work and, whilst this stepwise approach is an entirely practicable tactic for extending the range well beyond that used here, it lacks somewhat in convenience. On the other hand, a less sensitive system having considerably greater range but being of adequate displacement-sensitivity for this type of application could be constructed using identical optical principles.

PM MacKenzie
17th March 2007

FIG1

Click here to download high resolution image

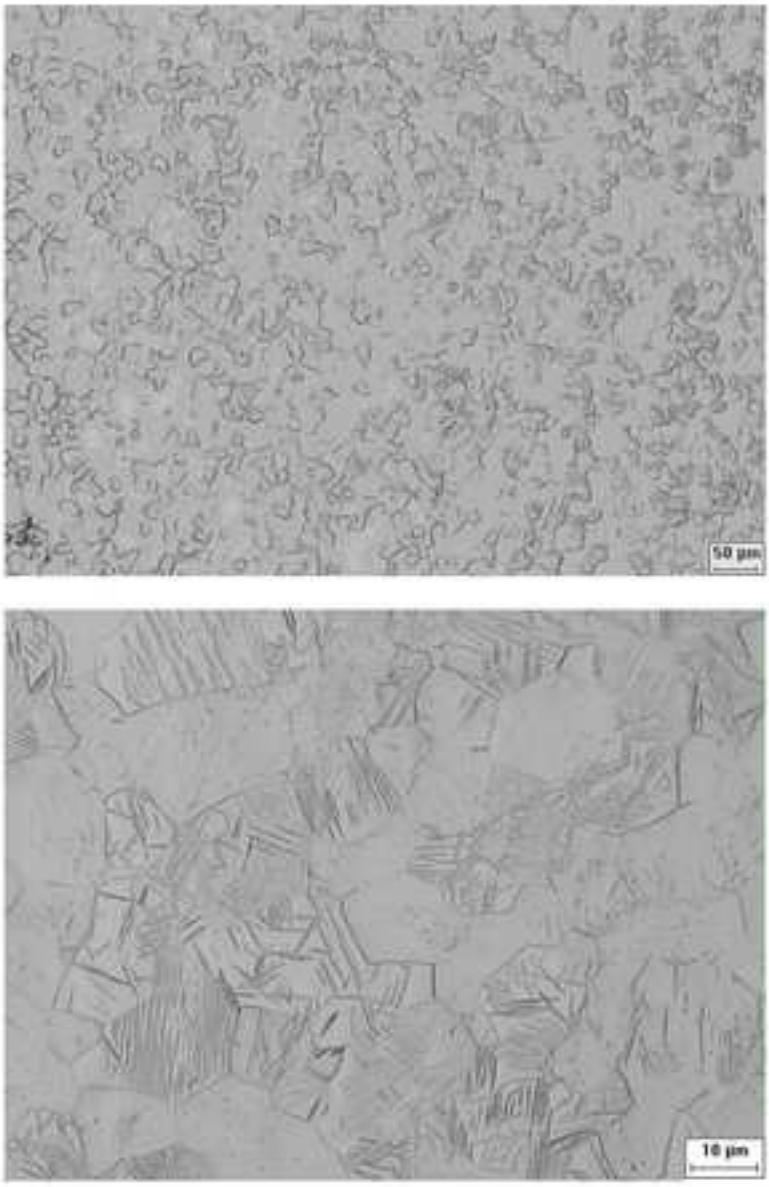

FIG2

Click here to download high resolution image

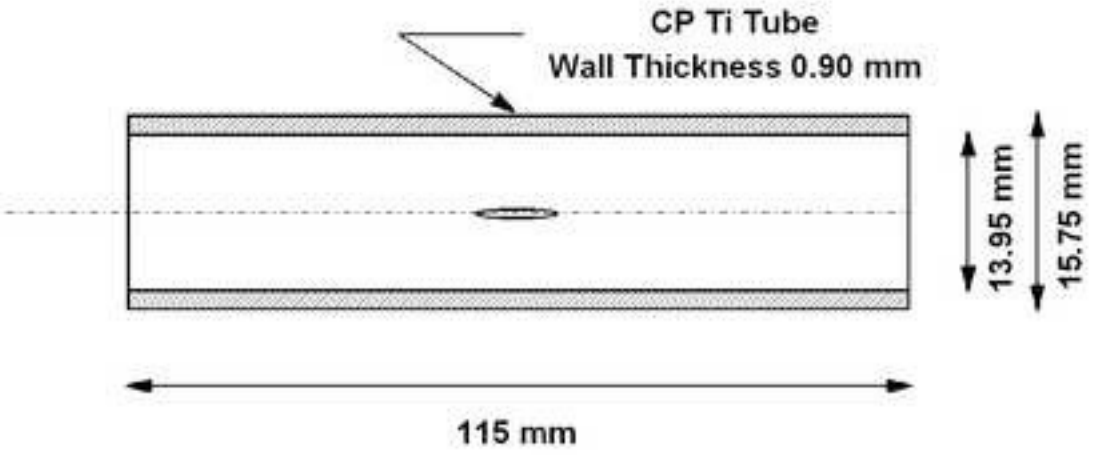

FIG3
Click here to download high resolution image

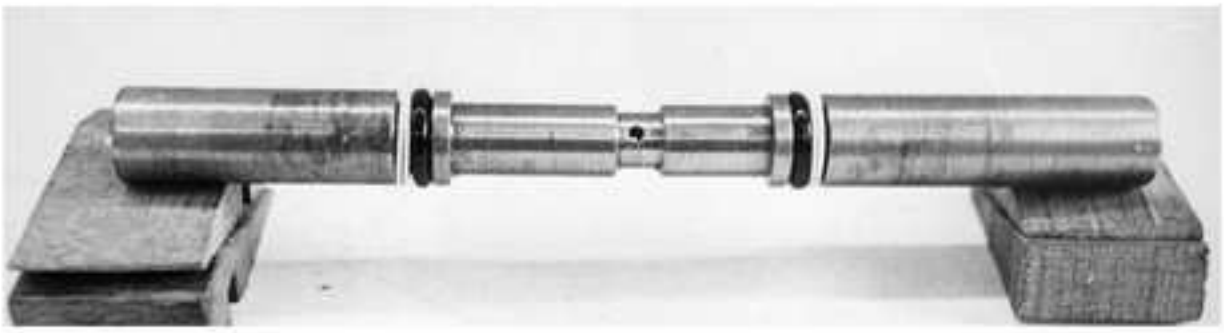

FIG4
Click here to download high resolution image

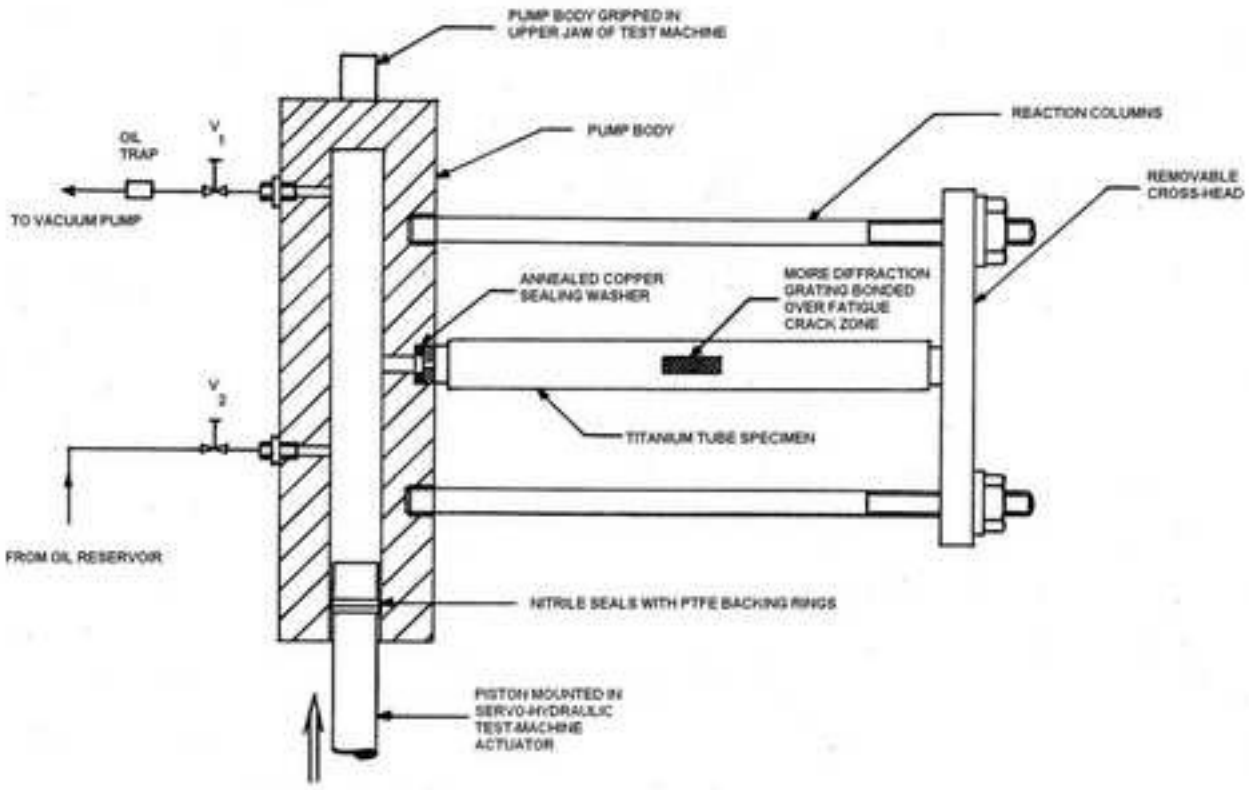

FIG5

Click here to download high resolution image

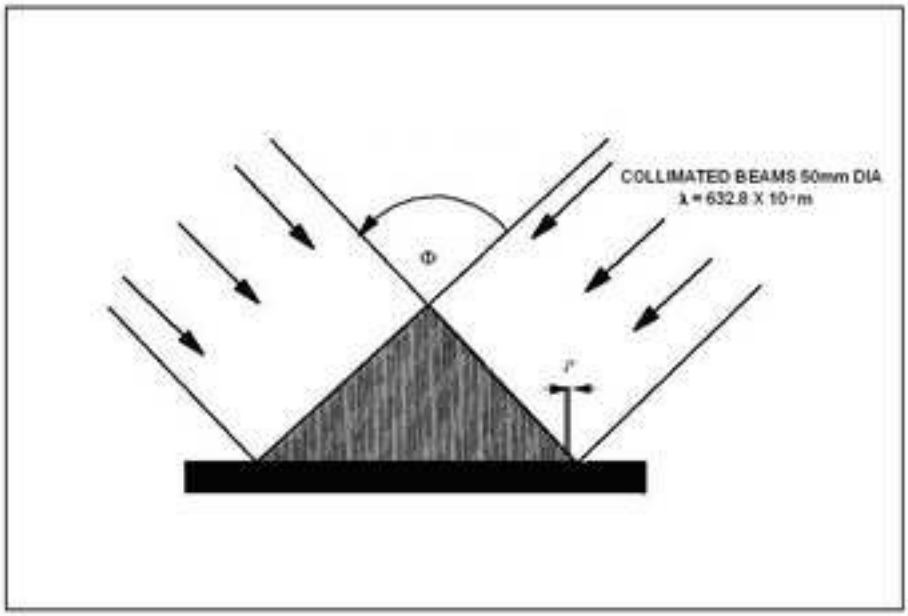

FIG6

Click here to download high resolution image

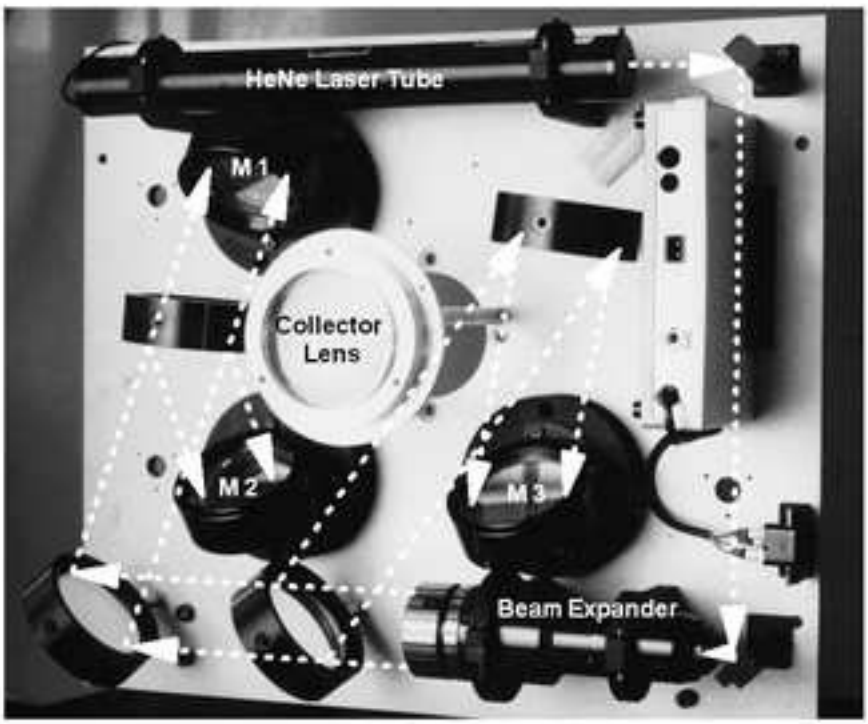

FIG7
Click here to download high resolution image

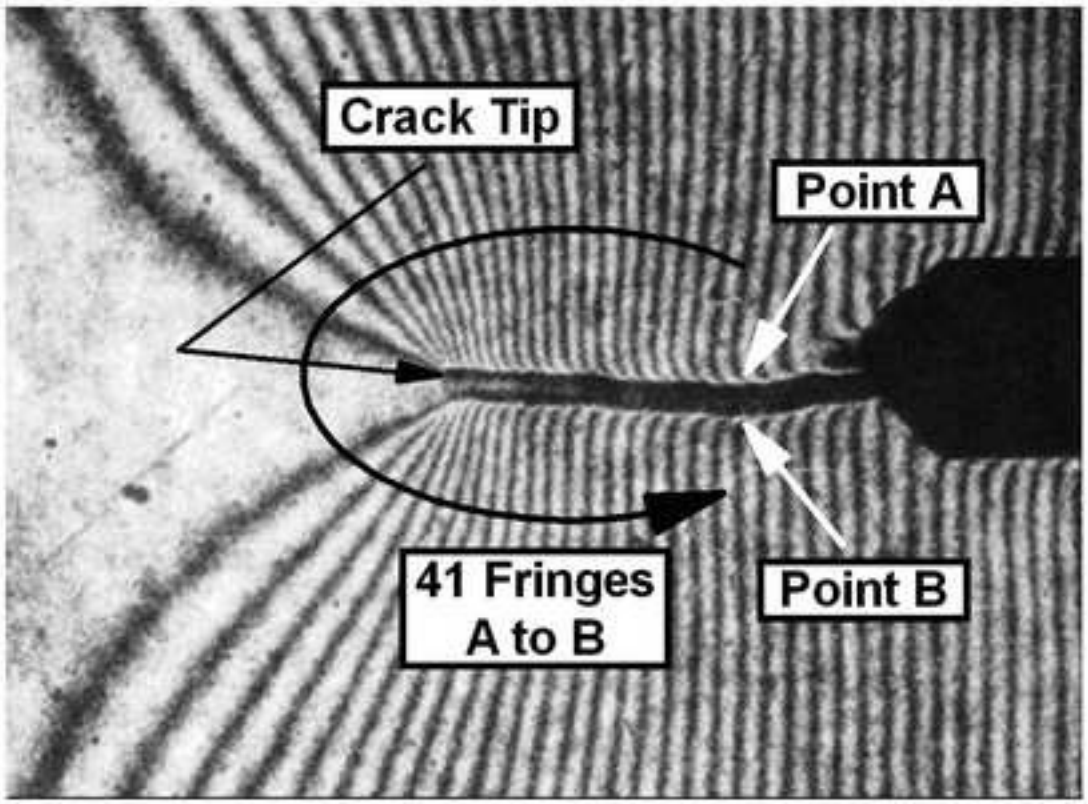

FIG8A

Click here to download high resolution image

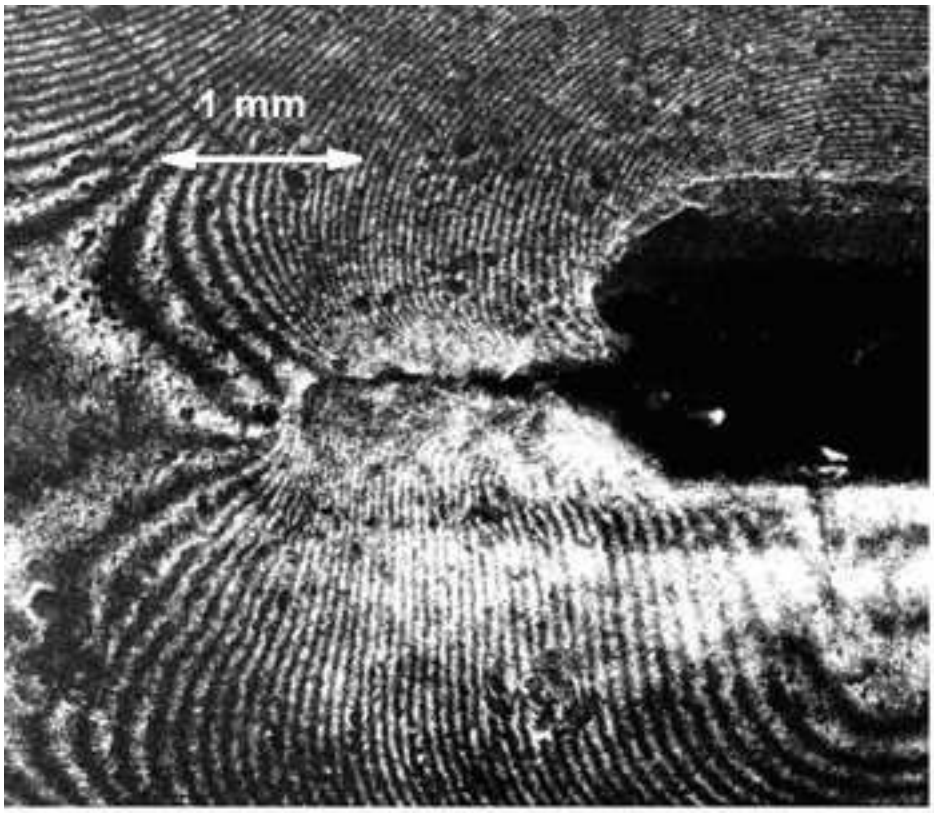

FIG8B

Click here to download high resolution image

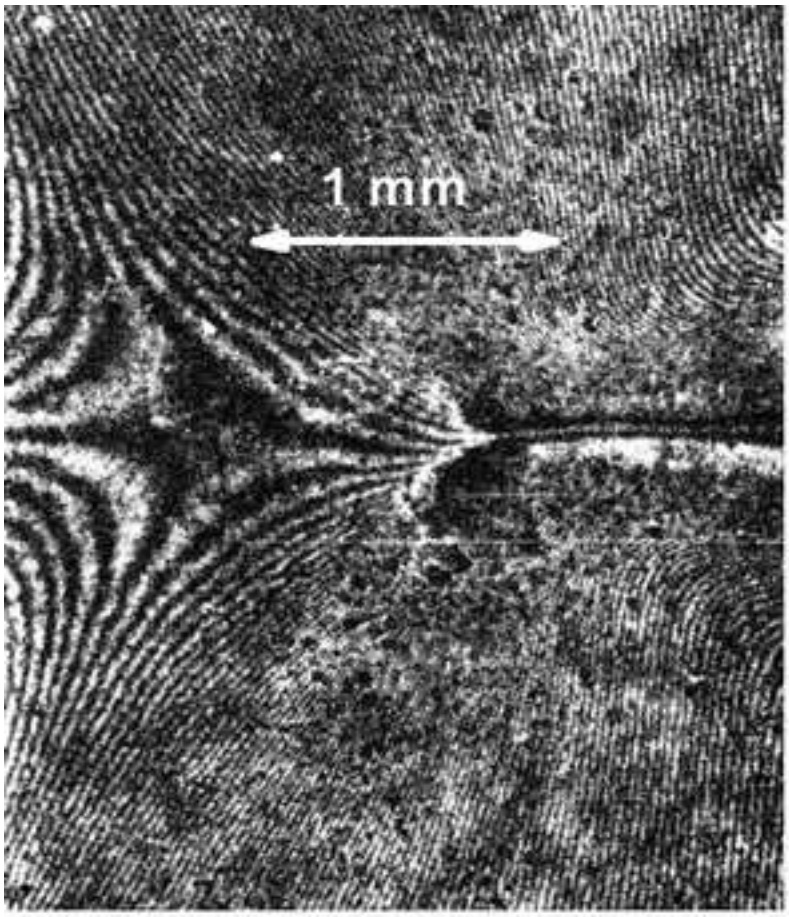

FIG9
Click here to download high resolution image

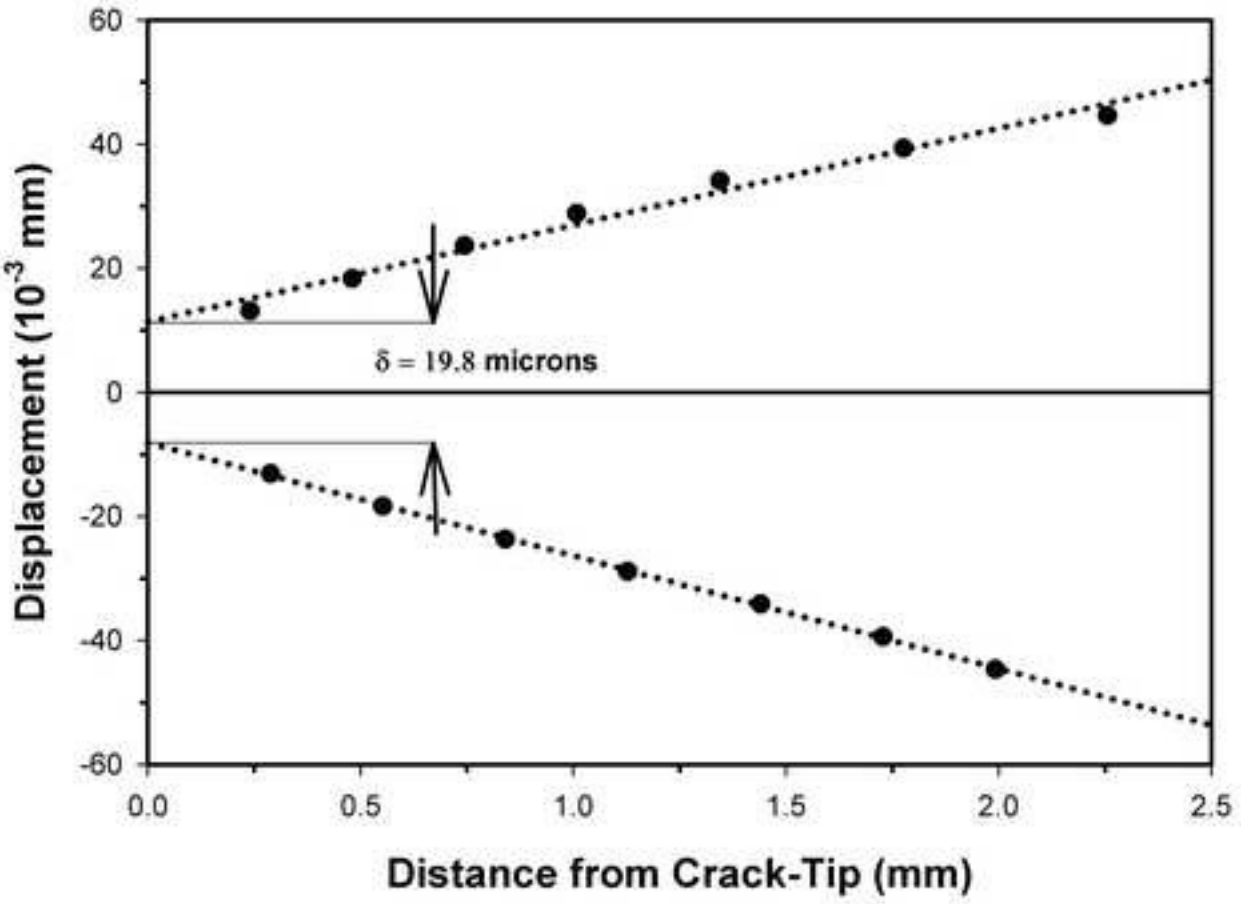

FIG10A

Click here to download high resolution image

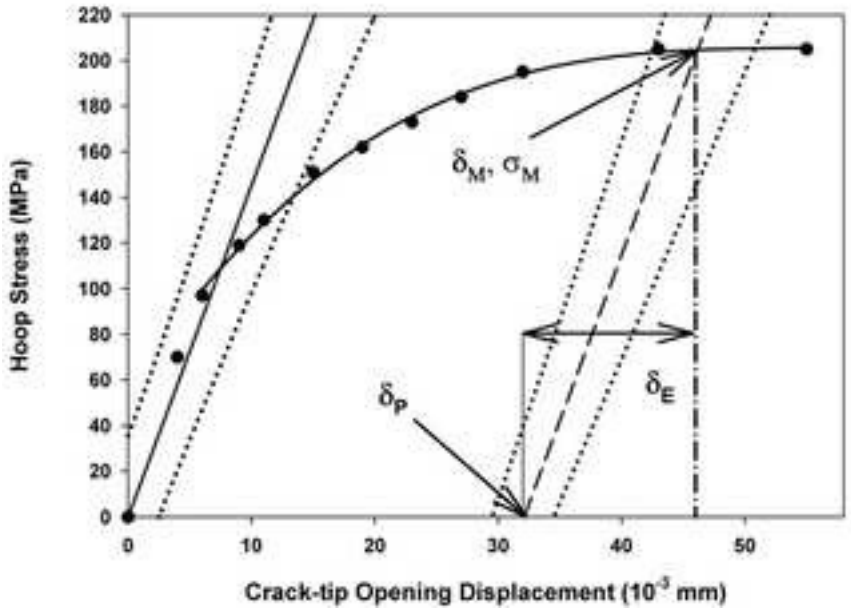

FIG10B

Click here to download high resolution image

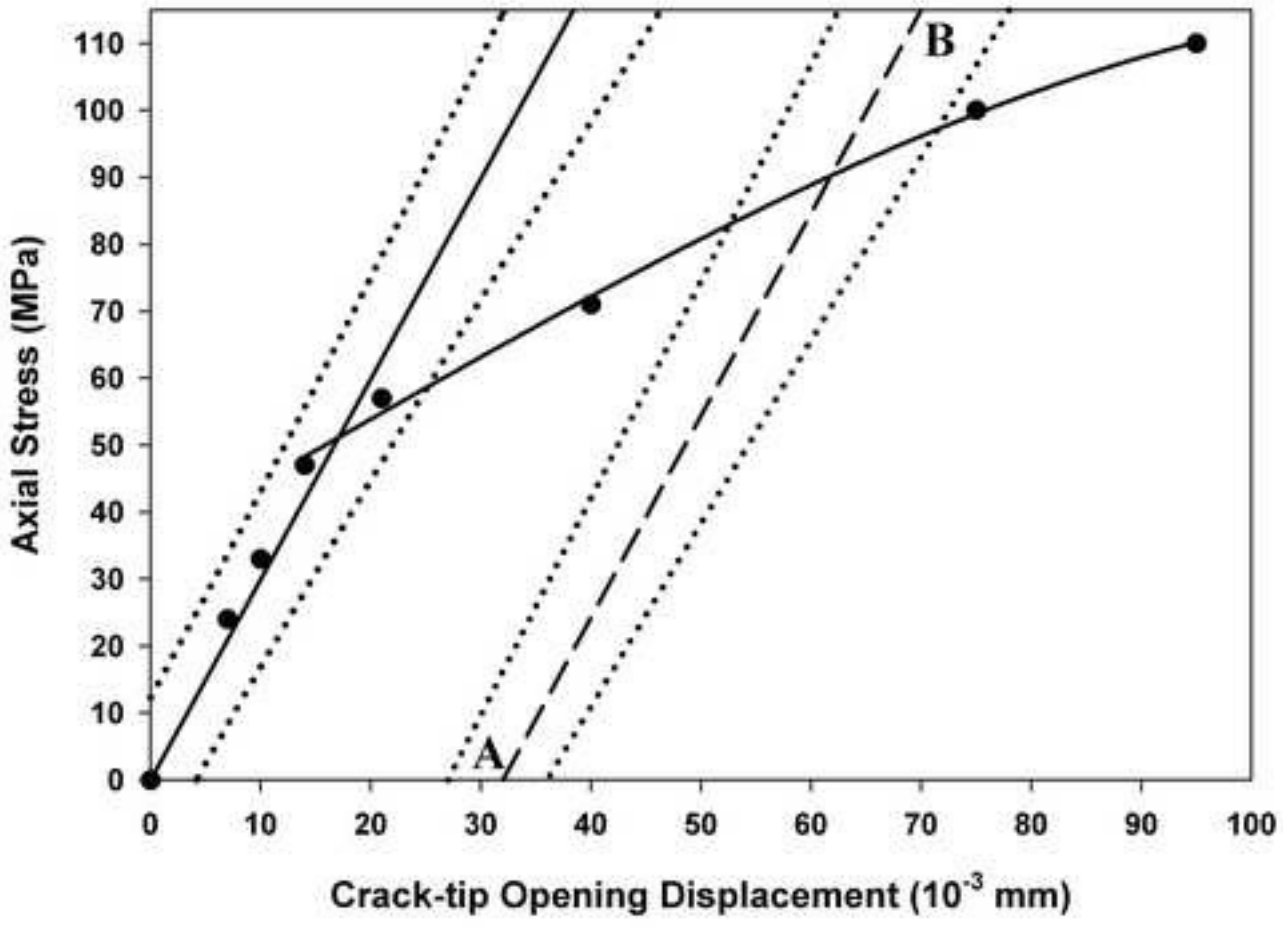

Table1

TABLE 1

Chemical Analysis of Commercially Pure Titanium Tube Specimens

Element	Ti	O_2	Fe	N_2	C	H_2
Wt %	Balance	0.11%	0.03%	0.007%	<0.010%	0.004%

Table2

TABLE 2

Results of Tests to Failure of Un-cracked Tubes

	0.2% Proof Stress MPa	Ultimate Stress MPa	Elongation, or Diametrical Strain at Failure %
Hoop Loading	**484**	**966**	**59**
Axial Tensile Loading	**397**	**627**	**32**

Table3

TABLE 3

Comparison of Some Characteristics of Fracture Performance for Axial and Circumferential Crack Orientations

	K MPa $m^{1/2}$	δ_P x 10^{-6} m	δ_M x 10^{-6} m	δ x 10^{-6} m
AXIAL CRACK	$K_{APP} = K_M =$ **55**	**32**	**46**	**46**
CIRCUMFERENTIAL CRACK	$K_{APP} = K_M$ **for axial crack = 55**	**-**	**-**	***96***
AXIAL CRACK	**55**	**32**	**46**	**46**
CIRCUMFERENTIAL CRACK	***43***	$\delta_P = \delta_P$ **for axial crack = 32**	**-**	***62***
AXIAL CRACK	**55**	**32**	**46**	**46**
CIRCUMFERENTIAL CRACK	***38***	**-**	**-**	$\delta = \delta_M$ **for axial crack = 46**